

Article

Economic and Ultrafast Photocatalytic Degradation of Orange II Using Ceramic Powders

Dikra Bouras¹, Abla Mecif¹, Abdelhamid Harabi², Régis Barillé^{3,*} , Abdel hakim Mahdjoub⁴ and Mourad Zaabat¹

¹ Laboratory of Active Components and Materials, University of Oum El Bouaghi, Oum El Bouaghi 04000, Algeria; bouras.dikra@yahoo.fr (D.B.); mecifabla@yahoo.fr (A.M.); zaabat@hotmail.com (M.Z.)

² Ceramics Lab, Mentouri University of Constantine, Constantine 25000, Algeria; harabi52@gmail.com

³ MOLTECH-Anjou, Université d'Angers/UMR CNRS 6200, 2 bd Lavoisier, 49045 Angers, France

⁴ Laboratory of Materials and Structure of Electromechanical Systems and Their Reliability, Faculty of Sciences and Technology, University of Larbi Ben M'Hidi, Oum El Bouaghi 04000, Algeria; Mahdjoub@umc.edu.dz

* Correspondence: regis.barille@univ-angers.fr

Abstract: Different percentages of CuO and ZnO were added into a local kaolin ceramic-based powder (DD3) with and without ZrO₂. The modified powders were first characterized, then, a test for the photocatalytic degradation of dyes with orange II (OII) was carried out. The DD3 powders that were obtained with the addition of ZrO₂, ZnO, and CuO, were prepared by two different methods and have shown a large and very fast photocatalytic activity. Discoloration ratios of about 93.6% and 100% were reached after 15 min and 45 min, for CuO and ZnO respectively. Finally, an alternative photocatalysis mechanism, based purely on chemical reaction processes, is proposed. The photocatalysis results with modified powders are compared with the results obtained with thin films, made with the same materials.

Keywords: Mullite; Zircon; Co-precipitation method; photocatalysis; ZnO/CuO; degradation rate



Citation: Bouras, D.; Mecif, A.; Harabi, A.; Barillé, R.; hakim Mahdjoub, A.; Zaabat, M. Economic and Ultrafast Photocatalytic Degradation of Orange II Using Ceramic Powders. *Catalysts* **2021**, *11*, 733. <https://doi.org/10.3390/catal11060733>

Academic Editors: Alaa Khalil, Jae-Woo Choi, Keunsu Choi and Ewa Kowalska

Received: 13 May 2021
Accepted: 10 June 2021
Published: 14 June 2021

Publisher's Note: MDPI stays neutral with regard to jurisdictional claims in published maps and institutional affiliations.



Copyright: © 2021 by the authors. Licensee MDPI, Basel, Switzerland. This article is an open access article distributed under the terms and conditions of the Creative Commons Attribution (CC BY) license (<https://creativecommons.org/licenses/by/4.0/>).

1. Introduction

In recent years, the world has seen a large population growth and an increase in huge modern industries. These factors significantly enlarge the percentage of everyday disposed wastes. Most of this waste, one way or another, begins or ends in rivers, leading to terrible pollution. In order to face this problem, ceramics have been used as a raw material for the purification of water [1,2]. The choice of this raw material was motivated by the large availability of ceramics in nature at a low cost, particularly in Algeria. Many countries in the world have abundantly these raw materials such as calcium carbonates (CaCO₃), dolomite (CaCO₃.MgCO₃), bones (natural derived hydroxyapatite (HA): Ca₁₀(PO₄)₆(OH)₂), kaolin, feldspar, and quartz. Many works have already been published for valorizing these native raw materials for the production of ceramic membranes [3–5]. Besides these studies, other interesting works were also published on both advanced ceramics [6,7] and bio-ceramics [8]. All of these publications are closely related to the goal of this present work and clearly draw attention to possible multifunctional applications.

Since ceramic filters are generally constituted of a thick support (2000 μm) with mono or multi thin membranes (from 10 to 40 μm for each one), the replacement of the more expensive base materials, mentioned above, by other cheaper raw materials used in supports (which constitute about 99% of the filter mass), is significantly important. Consequently, considering this goal, ceramic based supports [9], and/or other supports [10,11], were applied for the elaboration of low-cost ceramic microfiltration membranes applied to the sterilization of plant tissue culture media [12]. Concerning bio-ceramic publications [13], a

lot of low-cost materials were also employed, based on the abundantly available raw materials previously mentioned above. More recently, HA (Hydroxyapatite) based ceramics were fabricated from natural HA using an original milling system, carried out by A. Harabi and E. Harabi [14]. In this study, a particular desktop wet milling setup has been proposed to obtain sub-micron sized HA powders. In addition, a simple and instant visual approach of the animal bone age classification is proposed.

Generally speaking, there are two main filtration methods of polluting (or contaminating) waste materials. The first one consists of physical filtration of polluting particles (ceramic membrane filtration) using economic and abundantly raw materials [15,16]. By contrast, the second method allows (based on the photocatalytic activity) the discoloration or degradation with powders by chemical reactions. Opportunely, the zone of Jebel Debbagh, located in Guelma in the east of Algeria, is among the richest areas for kaolinitic clays of different types. Therefore, kaolinitic clays, named DD3, have been selected in the present study.

However, this raw material is not sufficient alone for a fine filtration. Numerous studies have shown that by adding several elements, an increase in the degree of its efficiency can be observed [17,18]. Water purification using zinc oxide (ZnO) is one of the most popular materials. In this work, an optimal material for filtration was fabricated. The ceramic is the main material and other contents were mixed. A content of 38 wt% ZrO_2 is the best value for an optimal pore diameter and is added to the DD3 kaolinitic clay. These two materials were mixed and treated at 1300 °C for 2 h. This step is performed for a composite of mullite and zircon with a rate of suitable porosity of 33% [19]. The resulting ceramic is used as a photo-reactor in the goal to absorb impurities from a polluting solution. The obtained absorption rate was adequate but not satisfactory. In order to improve this rate, additive materials that are also available at a low cost were used. These additives are acetates, copper, and zinc oxides (depending on the method of preparation). These two oxides are known for their stimulation of interactions in the aqueous solution [20]. In addition to this feature, ZnO is known for its high photosensitivity, stability at high bandwidth [21] and its ability for degradation of many environmental contaminants (a good photocatalyst) [22]. The copper oxide and zinc oxide are non-toxic p-type and n semiconductors, respectively. Their energy band gap is $E_g = 1.2$ eV for CuO and $E_g = 3.4$ eV for ZnO [23,24]. In addition, these two oxides may improve the properties of the catalyst. These results have shown their efficiencies in several applications [25,26]. Indeed, once the oxides are prepared, their ions, whose role is to absorb existent impurities in dyes (for example orange II solution), allow the development of photocatalyst materials and lead to optimize the efficiency for depollution.

In this work, different methods are applied to the powder fabrication, namely co-precipitation and traditional mixture. The material is a kaolin-based material, functionalized with different oxides. The effects of these two different methods for the material preparation are tested for the photocatalysis of a dye. The efficiency of the photodegradation is studied and a mechanism is proposed. The results obtained show that the degradation of a dye (orange II (OII)) reached 94.4% for the use of powders prepared by the co-precipitation method, after about 45 min. For powders prepared by the mixing method, a degradation rate of 93.63% was obtained after 15 min. The addition of ZnO, which is mainly for the ceramics modified with ZrO_2 , increases the efficiency. The experimental results of the prepared ceramic-based materials for the degradation of a dye are compared with the thin film results made with the same materials and applied on different dyes for degradation.

2. Experimental Studies

2.1. Xray Diffraction

The powders produced by different methods of preparation were treated at 500 °C and characterized by X-ray diffraction (XRD). The obtained results are shown in Figure 1a–f. Figure 1a,b present DD3 ceramic powders prepared by a traditional mix, while Figure 1c,d

are related to the same ceramic prepared by a co-precipitation method. In addition to the peaks of the ceramic phases (mullite (JCPDS 15-0776), zircon (JCPDS 06-0266), zirconia (JCPDS 37-1484), and cristobalite (JCPDS 39-1425)), it is noted that on all the spectra there are suitable intensity peaks of ZnO, in particular for a content of 50 wt%. The diffraction angles of these peaks are as follows: 36.42° for DD3 (Figure 1e) and 36.24° , 36.35° for DD3Z (Figure 1f) are compared with JCPDS No.36-1451 file and a ZnO hexagonal phase of Wurtzite type was found. By contrast, it can be noted that for the spectra of the ceramic containing ZnO and CuO, the peaks characterizing copper oxide appear only for samples with 12.5 wt% and 5.35 wt%. For other samples (2.8 wt% CuO), there is no peak of CuO and this may be due to the weakness of the added oxide content that cannot be detected by the XRD [27]. It is also possible that this absence of peaks is due to the superposition of CuO peaks on other phases. The peaks of the XRD spectra slightly shift to lower angles (Figure 1a,c) and to the higher angles in the same Figure 1b,d. The addition of CuO contributes to a variation of the lattice parameters which results in a slight shift of the peaks. This can be also explained by a substitution of the atoms of the ceramic structure by the Cu^{2+} ions [28]. The results are presented in the Table A1 (Appendix E).

The comparison between the results obtained by the different methods of preparation shows that the peaks in the XRD spectra of samples prepared by co-precipitation are thinner than those of the samples prepared by the traditional mixing. Consequently, it is found that by using the co-precipitation method, finer grains are obtained.

The grain sizes of the powders can be extracted from the XRD data (see Appendix E. Table A1 in Appendix E gives the results for DD3 before and after addition of Zn and Cu and for DD3 + 38% ZrO_2 (DD3Z) after addition of Zn and Cu.

2.2. Scanning Electron Microscopy (SEM)/Energy Dispersive X-ray Spectroscopy (EDX)

The morphology of the catalyst material prepared by the *traditional mixing* method was studied by SEM (Figure 2). The size of the granules was not homogeneous because of the differences between the ceramic materials and the additive oxides. In the SEM images shown in Figure 2a,c, there is a clear change in the shape of granules after the addition of ZrO_2 into the DD3 clay material. Moreover, it was observed that there was an increase in the number and in the average size of pores. The value of the pore sizes changed from 50 nm (without ZrO_2 addition) to 292 nm (with ZrO_2 addition). The addition of both zinc and copper oxides into the two types of ceramics has contributed significantly to the increase in the percentage of pores within the granules and induced the capture of a larger number of impurities in the dye. These two oxides also changed the morphology of the DD3Z material and led them to become similar to flake-like structures with more pores, compared to raw DD3. The raw material maintained its characteristics with only a small increase in the number of pores. The compositional elements of these powders by the EDAX analysis confirmed the presence of Zn and Cu metals or oxides in the DD3 and DD3Z clays (Figure 3).

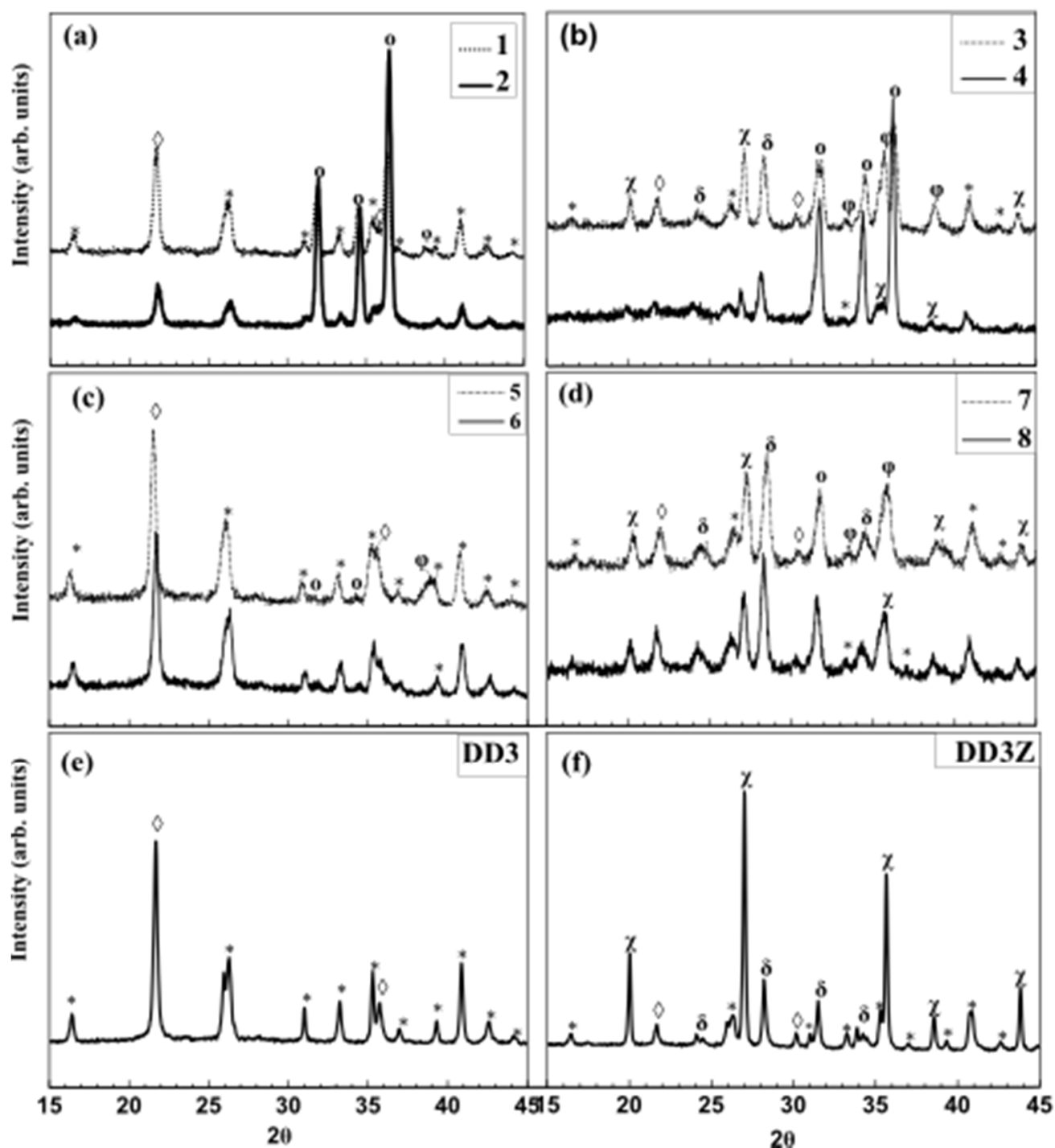


Figure 1. XRD spectra of powders treated at 500 °C prepared by the traditional mixing method (a,b) and co-precipitation method (c,d). χ : Zircon (ZrSiO_4), δ : Zirconia (ZrO_2), \diamond : Cristobalite (SiO_2), \ast : Mullite ($3\text{Al}_2\text{O}_3 \cdot 2\text{SiO}_2$), \circ : ZnO and φ : CuO. (All of the additional ratios are given in weight percentage). The spectra of the initial clay DD3 (e) and modified DD3 with ZrO₂ is shown for comparison (f).

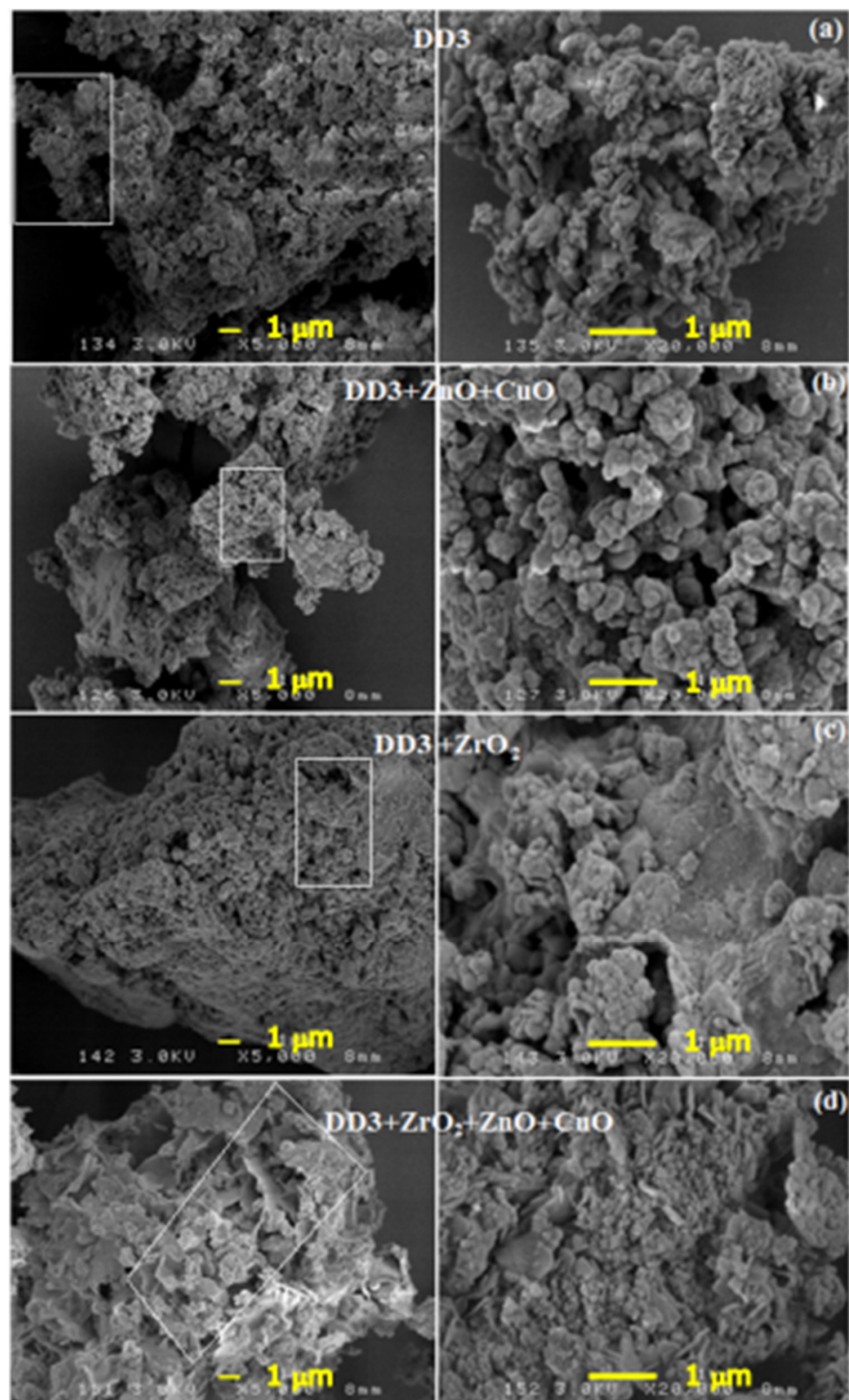


Figure 2. SEM images of DD3 (a), DD3+ 14.28 wt% ZnO + 5.37 wt% CuO (b), DD3 + 38 wt% ZrO₂ (c), and DD3 + 38 wt% ZrO₂+ 14.28 wt% ZnO + 5.37 wt% CuO (d).

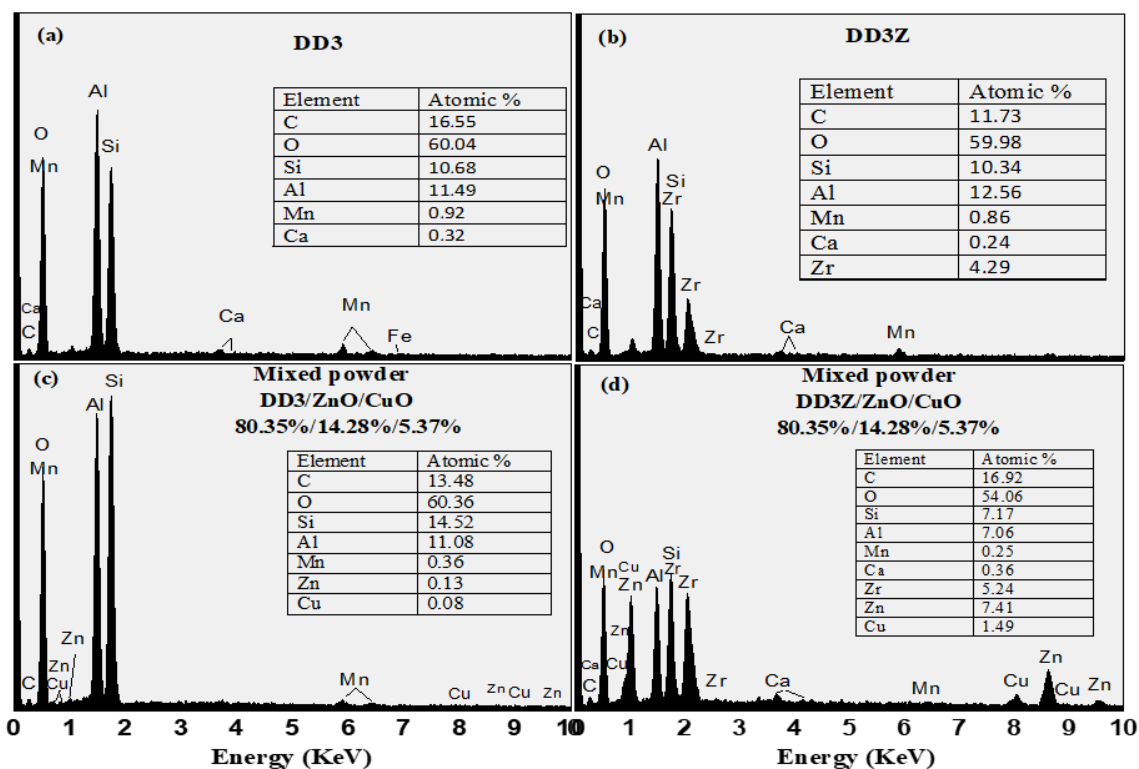


Figure 3. EDX analysis of catalysts showing composition of elements in table inset (all of the additional ratios are given in weight percentage). (a) DD3, (b) DD3Z, (c) DD3 + (14.28% ZnO—5.37% CuO), (d) DD3Z + (14.28% ZnO—5.37% CuO).

2.3. Vibrational Spectroscopy

In order to obtain a better characterization of the chemical sample compositions and interactions affecting the sample properties, the IR technique was used for the characterization of the obtained powders. This technique is frequently used to study structures, compositions, and chemical properties of materials. The obtained results by IR spectroscopy are presented in Figure 4. Several absorption bands in the wavelength range, from 400 to 2000 cm^{-1} , are clearly identified.

By comparing the IR spectra with no-addition and with different percentages of additions in the powders, sintered at 500 °C for 2 h, using two different methods of preparation, it can be seen that each of the spectra present an obvious phase. All spectra of powders without additional compounds correspond to the Mullite-Cristobalite (DD3) or the Mullite-Zircon (DD3Z) composite. The results of the analysis are complementary to the XRD results. Seven absorption peaks in both compounds are observed at 615, 735, 1086, and 1159 cm^{-1} . They are related to the process of forming the mullite present among them [29]. By comparing these results with the results obtained in the literature, the absorption bands at 615 and 1159 cm^{-1} are assigned to vibrations of the Al–O bond, while the 1086 cm^{-1} represents the Si–O bond. One can additionally notice that the appearance of the absorption band at 466 cm^{-1} characterizes O–Si–O bending vibrations (ν_2) [30]. Three absorption lines at 553, 735, and 834 cm^{-1} have a special association with Si–O–Al [31]. The cristobalite was assigned to a S–O stretching, appearing at 788 cm^{-1} value [32]. The reduction in the spectrum value was observed with the addition of zirconium oxide and is increased at 885 cm^{-1} . However, in this special case of the SiO_4 group (ν_3), the presence of the ZrSiO_4 phase is observed [33].

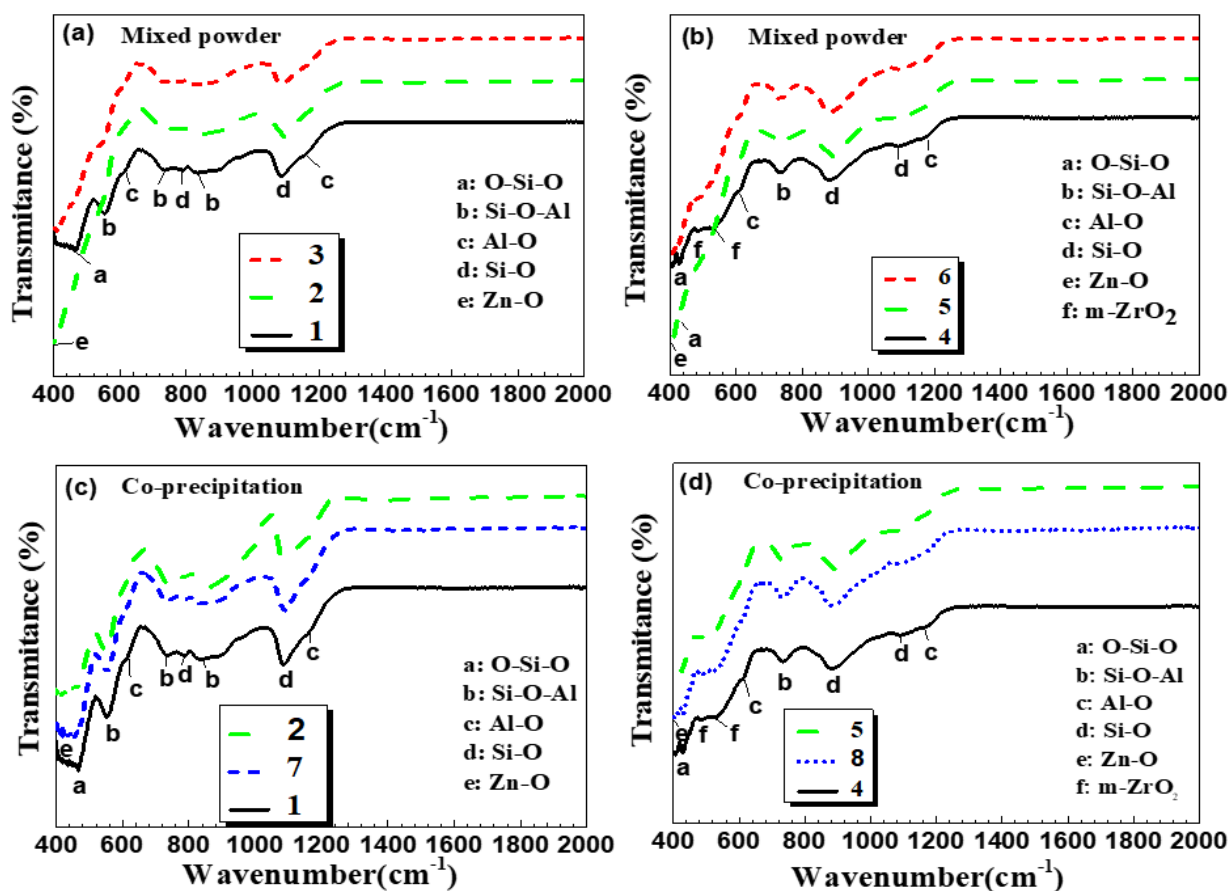


Figure 4. Infrared spectra of the catalysts (a,b) mixed power method, (c,d) co-precipitation method with (1) DD3, (2) DD3+ 28 wt% CuO + 2.8 wt% ZnO, (3) DD3 + 14.28 wt% ZnO + 5.37 wt% CuO, (4) DD3Z, (5) DD3Z+ 28 wt% CuO + 2.8 wt% ZnO, (6) DD3Z+14.28 wt% ZnO + 5.37 wt% CuO, (7) DD3+ 25 wt% ZnO + 12.5 wt% CuO, and (8) DD3Z + 25 wt% ZnO + 12.5 wt% CuO.

The results of XRD measurements have also previously revealed the surplus or residual quantity of the added monoclinic ZrO_2 oxide (Figure 1b,d,f). The absorption band for the latter is localized at 484 cm^{-1} in the IR spectrum of Figure 4b. For powders made by the traditional mixing method (Figure 4a,b), the absorption curve changed in the $400\text{--}590\text{ cm}^{-1}$ range. A decrease in the intensity of the ZnO absorption line of the spectrum is very clear at 408 cm^{-1} and corresponds to the Zn-O vibration. In the same spectral range, the transmission spectra decreased when oxides were added (ZnO and CuO) into the ceramics powder [34]. A change in the peaks of the transmission spectra was observed between DD3 + 14.28 wt% ZnO + 5.37 wt% CuO and DD3 or DD3Z + 14.28 wt% ZnO + 5.37 wt% CuO and DD3Z. This result has not been experienced with the co-precipitation method (Figure 4c,d), where the same absorption curve is maintained even after the addition of each compound with the emergence of a band at 424 cm^{-1} characteristics of ZnO.

By comparing the two methods, the spectrum of zinc oxide with the appearance of the absorption bands by the mixing method can be clearly distinguished. This will be confirmed later by a photocatalytic application, where the mixing method was more effective than the co-precipitation method.

2.4. Optical Analysis

The optical analysis was performed for the DD3, DD3Z and DD3/ DD3Z + (ZnO (14.28%), or CuO (5.37%)) samples. The measurements were performed in the wavelength range of $200\text{--}900\text{ nm}$. The results are shown in the Figure 5. It can be noted that the absorbance is maximal for the sample DD3 + ZrO_2 (DD3Z). The presence of CuO and ZnO

in the DD3 and DD3Z clay improved the absorbance in a remarkable way. The absorbance decreased with the addition of ZrO_2 in the clay, which can be explained by the formation of the $ZrSiO_4$ component, which is characterized by a great optical reflection. The increase in the photocatalytic effect is mainly attributed to the increase in the reaction surface (grain porosity). With this goal in mind, the addition of ZnO (14.28 wt%) and CuO (5.37 wt%) appears to give a good absorbance with the two added chemical compounds (ZnO and CuO) that match their gaps [35]. It is noted that zinc oxide absorbs below 375 nm, and copper oxide has a low gap and absorbs almost the entire visible leading to a black powder.

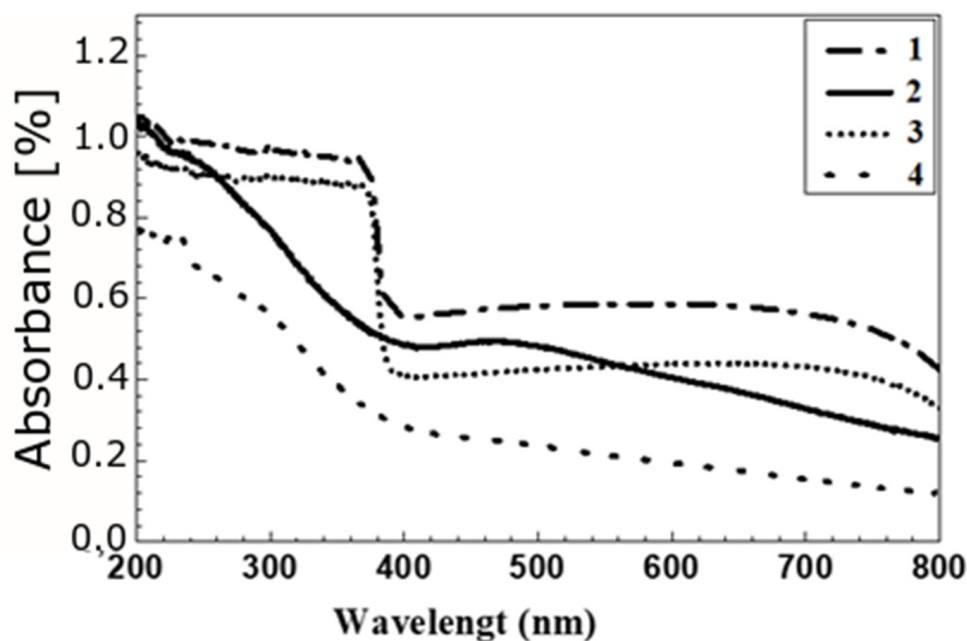


Figure 5. UV-Vis Absorption Spectra of the catalysts. (1) DD3 + 14.28 wt% ZnO + 5.37wt% CuO, (2) DD3, (3) DD3Z + 14.28 wt% ZnO + 5.37wt% CuO, (4) DD3Z (DD3 + 38%ZrO₂).

2.5. Photocatalytic Performance

With the goal of developing practical applications, the prepared samples were tested for purification of contaminated solutions. This study was carried out by measuring the degradation of orange II as a function of time. The dye was chosen because it represents more than 50% of the world production of coloring matter [36]. It is initially non-biodegradable and resistant to bacterial attacks in aqueous media [37].

By contrast, this application was previously carried out on powders prepared by both conventional mixing and co-precipitation methods. These powders are DD3 and DD3Z without and with different contents of ZnO and CuO. Figure 6 represents the visible UV spectra obtained for samples prepared by a traditional mixing. It is noted that for DD3 and DD3Z powders (Figure 6a,b), the degradation of orange II reaches 42% and 60.3% for 7 h and 2 h, respectively. These values are remarkably improved by the addition of ZnO mainly for DD3Z (Figure 6c–f), for which the purification percentage reached very high rates during short periods. For example, a complete purification (98.9%) of an OII solution was almost achieved during 15 min with the addition of 50 wt% ZnO to DD3Z. The same result was obtained with DD3 + 50 wt% ZnO with a degradation time of 30 min.

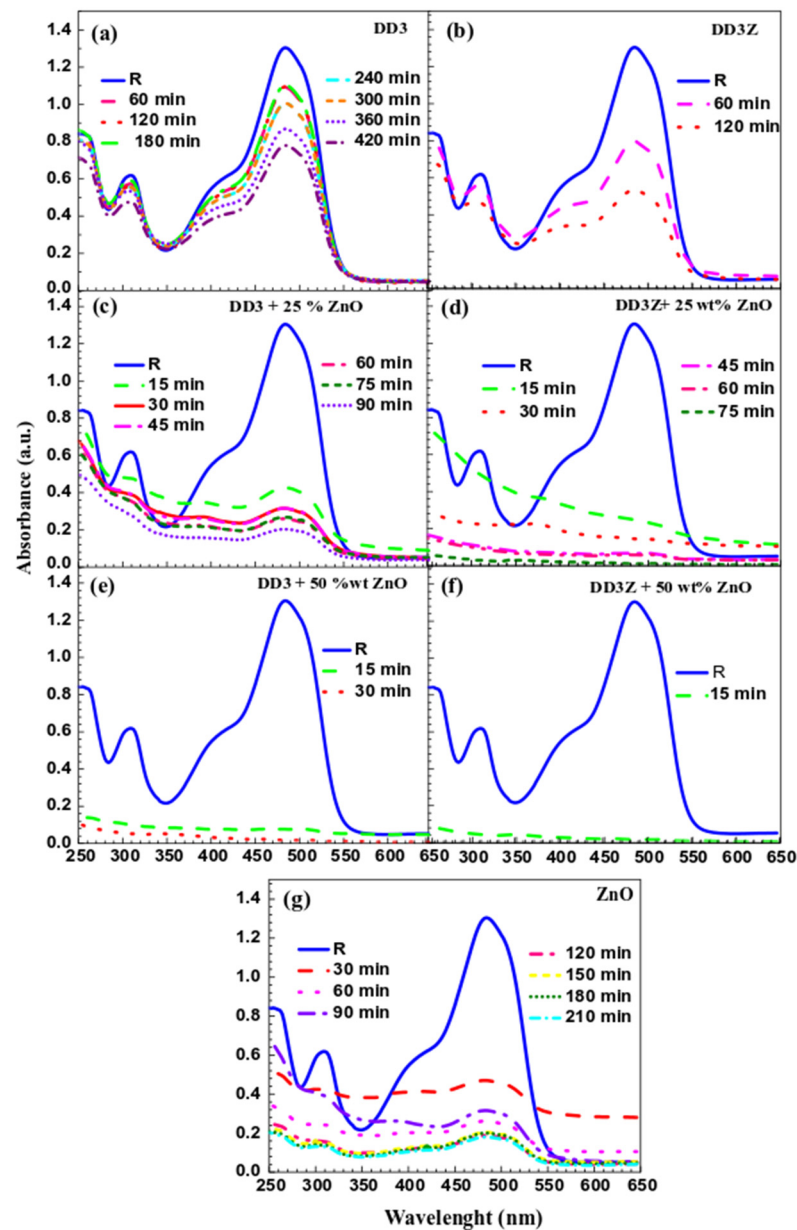


Figure 6. UV spectra showing the ZnO doping effect in the ceramic powder prepared by the traditional mix method and treated at 500 °C (degradation of OII ($\lambda_{\max} = 484$ nm) versus time) (all of the additional ratios are given in weight percentage). (a) DD3, (b) DD3Z, (c) DD3 + 25% ZnO, (d) DD3Z + 25% ZnO, (e) DD3 + 50% ZnO, (f) DD3Z + 50% ZnO, (g) ZnO. R = reference for OII.

The high rate of purification obtained with the samples was experienced with a ZnO content of 50 wt%. In order to reduce this content and to have samples where the ceramic material was dominant, another sample with addition of ZnO was used. These samples have the same efficiency for purification applications and were prepared following the same protocol (traditional mixing method).

The added material for this purpose was copper oxide (CuO) because of its positive properties in this domain of applications. The study was carried out with 5.37 wt% CuO and 14.28 wt% ZnO. Using UV-visible spectra, the obtained photocatalysis for these samples is represented in Figure 7. There is a remarkable improvement in the degradation rate for DD3-based samples (Figure 7a,c,e,g) when it is compared to the degradation time of DD3Z-based samples (Figure 7b,d,f,h). The degradation rate reached 82.4% for 30 min (Figure 7g) and 93.6% for 15 min (Figure 7h) for DD3 and DD3Z samples, respectively. It was also

found that by removing the UV lamp, the orange II degradation rate reached 89.52% for DD3 powders (Figure 8a) and 96.35% for powder DD3 + 38 wt% ZrO₂ powder in 45 min (Figure 8b).

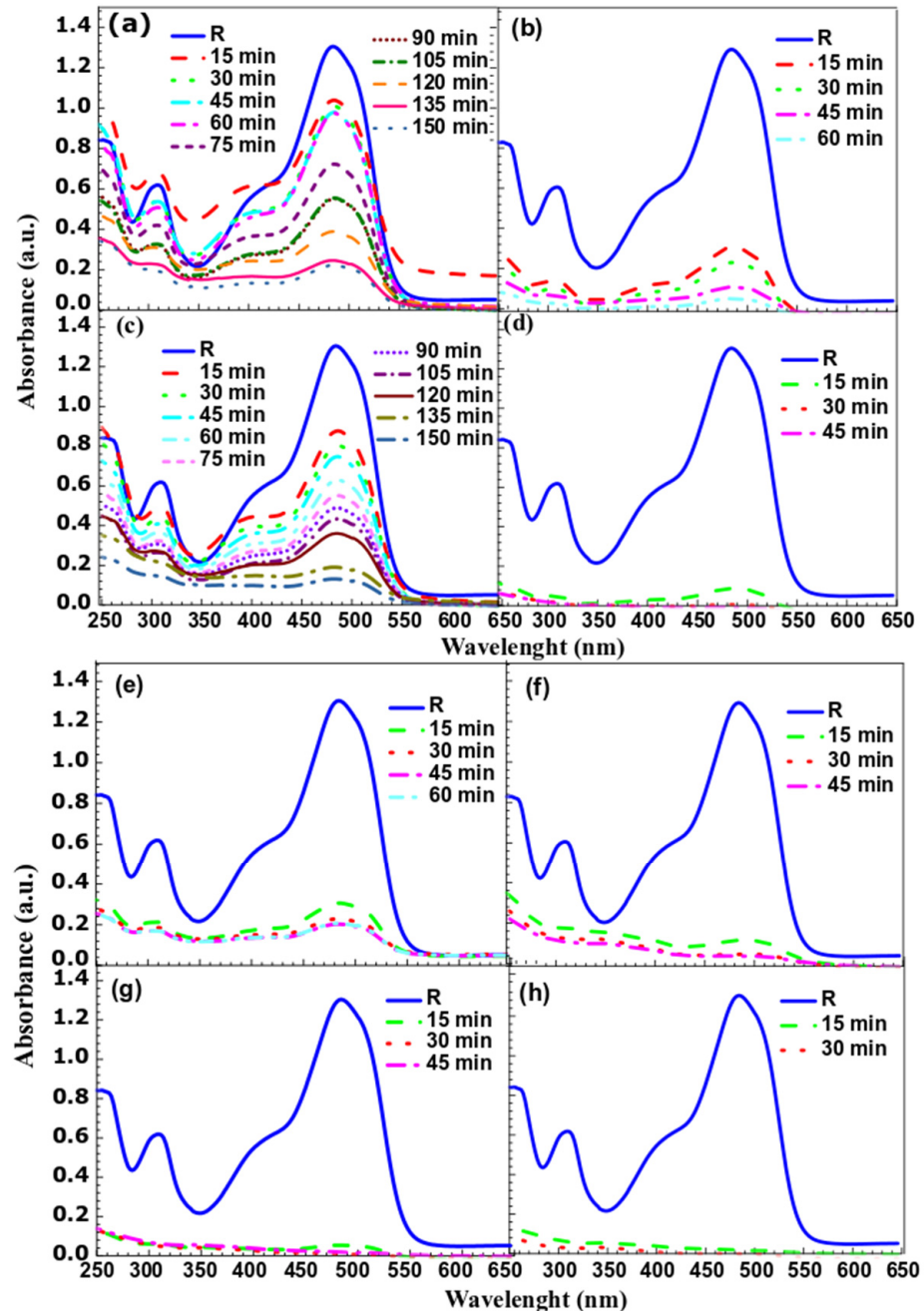


Figure 7. UV spectra showing the effect of the method for preparing ceramic powders doped and treated at 500 °C for degradation of OII ($\lambda_{\max} = 484$ nm), Co-precipitation method: (a) DD3 + 25 wt% Zn + 12.5 wt% Cu, (b) DD3Z + 25 wt% Zn + 12.5 wt% Cu, (c) DD3 + 28 wt% Zn + 2.8 wt% Cu, (d) DD3Z + 28 wt% Zn + 2.8 wt% Cu. Mixed powder method: (e) DD3 + 28 wt% ZnO + 2.8 wt% CuO, (f) DD3Z + 28 wt% ZnO + 2.8 wt% CuO, (g) DD3 + 14.28 wt% ZnO + 5.37 wt% CuO, (h) DD3Z + 14.28 wt% ZnO + 5.37 wt% CuO. R = reference for OII.

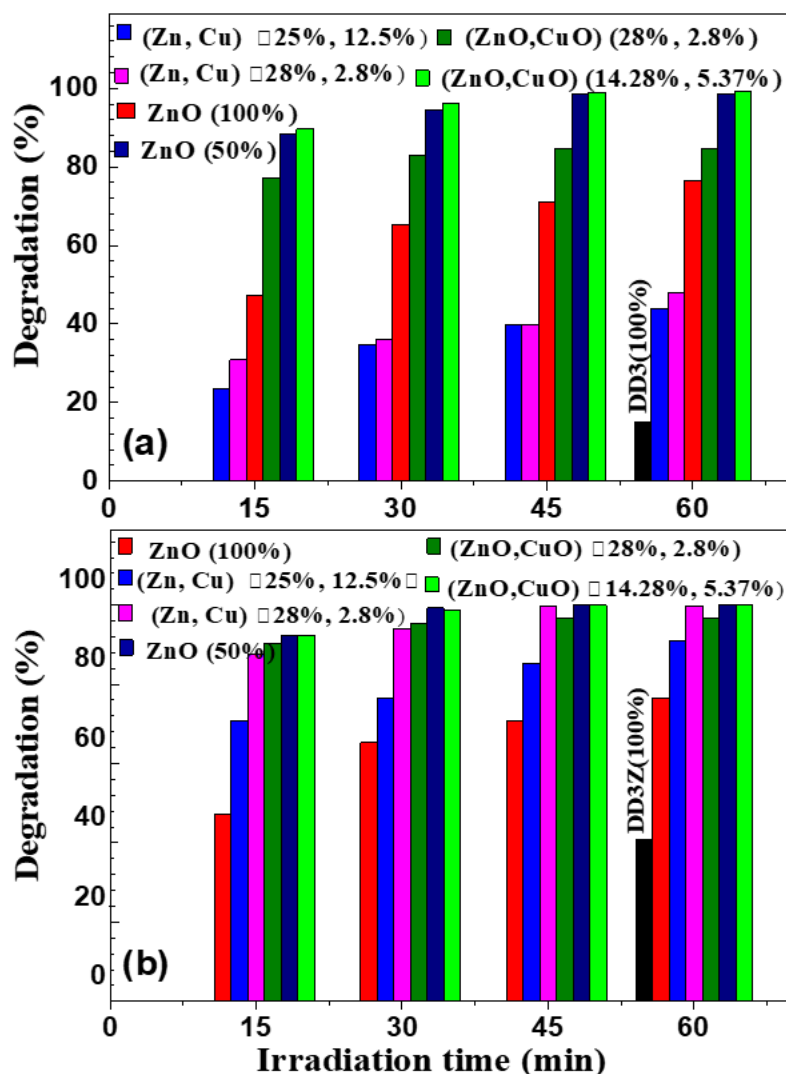


Figure 8. Percentage change of orange II photodegradation versus time for ceramic powders prepared by two methods: Traditional mix and co-precipitation for (a) DD3 and (b) DD3Z = DD3 + 38 wt% ZrO₂ (All the additional ratios are given in weight percentage).

For samples prepared by the co-precipitation technique, the obtained visible UV spectra are revealed in the Figure 7. DD3 or DD3Z clay samples were prepared with zinc acetate and copper acetate solutions. Significant results were obtained with the addition of 28 wt% ZnO and 2.8 wt% CuO. The purification percentage of orange II impurities reached 99.59% for a degradation time of 45 min with the DD3Z based samples (Figure 7b). Comparing with DD3-based samples, the degradation rate reached 84.13% for a time of 150 min (Figure 7a). The DD3Z based samples prepared with different methods had a suitable effect on the purification of orange II (Figure 8 and Appendix D).

Finally, all of the results concerning the degradation of OII with the prepared materials following two different methods are summed up in Figure 8. We observe that a very fast degradation of OII can be reached (less than 20 min.) even without lamp (see Appendix C). It is noted that there was no degradation of the orange II dye under UV light irradiation.

2.6. Mechanism of Photo-Catalysis

The photocatalysis mechanism is based purely on chemical reaction processes [38,39]. The samples tested for the photocatalysis were based on alumina-silicate ceramics with and without addition of ZrO₂. During the chemical reaction, SiO₂ and Al₂O₃ particles adsorb an amount of pollutants in the solution through the electrostatic attraction [40,41]

each doping material (ZrO₂, ZnO, CuO) under the light led to the creation of electron/hole. In the case of ceramics containing ZrO₂, the •OH radicals are generated by the creation of e⁻/h⁺ pairs and separated by the Al₂O₃ particles [42]. The radicals simultaneously act on the surface areas of the contaminant adsorbed on SiO₂ and Al₂O₃. Therefore, there is a possibility of degrading a large quantity of dye. However, this degradation is not fully satisfied as shown by Equations (A4), (A6), (A8) and (A13) in Appendix B [43].

In order to obtain good efficiency, we compared ZnO with and without CuO additions into the ceramics. It is noted that the number of holes increases in ceramics with the addition of ZnO and the addition of ZnO and CuO. This increase is due to the absorption of photons ($vh \geq E_g$); the mechanism for this phenomenon is explained by the scheme illustrated in Appendix B. The two semiconductors, CuO and ZnO, both added to the ceramics led to an accelerated degradation of OII. Consequently, this degradation is carried out by the p-n junction. After the absorption of the photon, a transfer of electrons can occur from the valence band of CuO (p-type) to the valence band of ZnO (n-type).

This is possible thanks to the work function of CuO, which is similar to the one of ZnO (5.3 eV) [44]. For a small amount of the two oxides (ZnO and CuO), the separation of electrons can be accelerated leading to an increase in holes. This electron separation plays a large role in the production of •OH radicals [45]. Moreover, the position of the ZnO edge of the conduction band is higher than that of ZrO₂. As a result, there is a rapid transfer of electrons from the conduction band (CB) of ZnO to the conduction band of ZrO₂, and this fast transfer prevents recombination. On the other hand, the transfer of holes may occur from the ZnO with the most anodic valence band to the cathode valence band of CuO (Equation (A3)). Potential edges CB of ZnO (-0.41 eV) and ZrO₂ (-0.38 eV) are negative with respect to the standard redox potential E[⊖] (O₂ / •O₂⁻) (-0.33 eV vs. NHE). In this case, electrons of ZnO and ZrO₂ can reduce O₂ to O₂⁻ (Equation (A4) and (A5)). However, this reaction is impossible for CuO, because of its positive CB edge potential (+0.71 eV) [46]. Thus, the process begins when the holes interact with water to produce hydroxide, and the electrons react with oxygen to induce a transparent color of the contaminated solution. The •O₂⁻ may then react with H₂O to form HO₂• and H₂O₂. Moreover, because of the position of the valence band edge of both ZrO₂ and ZnO oxides (+2.99 eV for ZnO and +3.22 eV for ZrO₂), there is potential to oxidize the dye to carbon dioxide and water with ZnO and ZrO₂ by the aforementioned holes [47,48]. The position values of the two semiconductors in zero charge point are calculated using the following relationships:

$$E_{VB} = X - E_e + 0.5E_g \quad (1)$$

$$E_{CB} = E_{VB} - E_g \quad (2)$$

where E_{VB} is the potential of the valence band edge, and E_{CB} is the potential of the conduction band edge, X is the electro-negativity value ($X_{CuO} = 5.81$ eV, $X_{ZnO} = 5.79$ eV, $X_{ZrO_2} = 5.92$ eV), E_e is the energy of free electrons at the level of hydrogen (~ 4.5 eV) and E_g is the band width of the semiconductor. The coexistence of the three oxides, ZrO₂, CuO, and ZnO, increase the rate of •OH in a very remarkable manner, compared to the case of only ZnO in ceramics. The formation of the holes is based on the chemical nature of ZrO₂, ZnO, and CuO. This may explain the high rate of orange II degradation in samples based on ceramics with three oxides compared to other cases.

2.7. Comparison with Thin Films

The photocatalysis results obtained with DD3 powder doped with different materials can be compared to thin films with the same materials (CuO, ZnO, ZrO₂). A. Katal et al. [49] reported the fabrication of a thin CuO film by a sputtering method and a thermal treatment for visible-light photocatalytic degradation of Methylene Blue (MB). The different surface structures and crystallinity of the different samples show the MB degradation with a minimum of 2 ppm after 200 min. The fabrication of CuO thin films through DC/RF magnetron sputtering technique [50] gives a similar result. Other studies with CuO includ-

ing CuO/zeoliteX [51], CuO/SiO₂ [52], heterojunction CuO–Cu₂O thin film [53] showed a maximum degradation after a similar period. CuO thin films contained 3D nanocubes [54] demonstrated a photodegradation activity by decomposing a 5 µM MB dye solution in 90 min under sun exposure. The ability of CuO thin films to degrade MB is attributed to the high density of exposed CuO nanocube surfaces, compared to other CuO thin film samples.

CuO/ZnO composite oxide thin films were prepared for the photocatalytic degradation of different dyes [55]. In all of the studies, the maximum degradation efficiency of nearly 90% was obtained after 120 min or 90 min in the best case. For example, D. S. Paz et al. [56] prepared CuO/ZnO coupled oxide films onto aluminum substrates by the electrodeposition method. The photocatalytic activities of the pure ZnO and coupled CuO/ZnO thin films with different CuO contents were compared. They showed that a pure ZnO film had a lower photocatalytic activity than the coupled CuO/ZnO films and that the photocatalytic activity of the CuO/ZnO films changed with the copper content. A maximum of degradation efficiency of 70% is reached after 300 min for CuO/ZnO. Another study showed that by coating ZnO with CuO to form CuO@ZnO core–shell catalysts [57], nitrophenols were degraded after 180 min.

ZrO₂ nano-thin films deposited at different substrate temperatures by the spray pyrolysis method [58] reached a maximum degradation of MB dye of 72.13% after 180 min of irradiation with sunlight only 30.82% degradation was observed after 30 min. The synthesis of ZrO₂ by the solution combustion technique or ZrO₂/TiO₂ mixed oxides [59]. Moreover, 80% degradation of a dye was observed in 2 h with a 25 ppm initial concentration. The best result was obtained with ZrO₂ calcined at 500 °C with about 85% degradation of methyl orange after 60 min. All the results are summed up in the Table 1 for comparison.

Table 1. Comparison between powder and thin film of dye degradation.

Material	Powder	Thin Film
DD3Z + 50 wt% ZnO	98.9% of a OII (15 min)	
DD3 + 50 wt% ZnO	98.9% of a OII (30 min)	
DD3 + 5.37 wt% CuO + 14.28 wt% ZnO	82.4% (30 min)	
DD3Z + 14.28 wt% ZnO + 14.28 wt% ZnO	93.6% (15 min)	
co-precipitation technique 28 wt% ZnO and 2.8 wt% CuO		
DD3 + 28 wt% ZnO and 2.8 wt% CuO	84% (150 min)	
DD3Z + 28 wt% ZnO and 2.8 wt% CuO	99.6% (45 min)	
CuO	Methylene Blue (MB) minimum 2 ppm after 200 min	
CuO/zeoliteX [52], CuO/SiO ₂ [53], heterojunction CuO–Cu ₂ O thin film		Methylene Blue (MB) minimum 2 ppm after 200 min
CuO/ZnO composite oxide thin films		90% (120 min)
ZnO with CuO to form CuO@ZnO core–shell		nitrophenols (180 min)
ZrO ₂ /TiO ₂ mixed oxides [58]		80% degradation of a dye was observed in 2 h
ZrO ₂ nano-thin films [59]		MB dye 72.13% (180 min)
ZrO ₂ calcined at 500 °C		85% methyl orange (60 min)

3. Methods

3.1. Materials

The raw materials based on DD3 with ZrO₂ (DD3 + 38 wt% ZrO₂) will be referred to in the study by DD3Z. In addition to the local clay used in this work, the following chemical compounds were added: zinc acetate [(CH₃COO)₂Zn·2H₂O; 99.5% purity], copper acetate [(Cu(CH₃COO)₂); 99.0% purity], copper oxide [CuO; 99.0% purity], zinc oxide [ZnO; 99.5% purity], sodium hydroxide [NaOH; 96.0% purity], and orange II (C₁₆H₁₁N₂NaO₄S) for the application. The chemical compositions of both DD3 kaolin and ZrO₂ have already been presented elsewhere [60], with the influence of ZrO₂ content (wt%) on the open porosity ratio of compact clay materials sintered at 1400°C for 2 h. The value of 38% gives the best open porosity.

3.2. Characterization Techniques

The crystal structure of the powder particles was identified by X-ray diffraction (XRD; Bruker AXS-8D, Karlsruhe, Germany) using a Cu Kα (λ = 1.5406 Å) radiation. To examine the microstructure composition, the scanning electron microscopy (SEM; JSM-6301F, Tokyo, Japan) and energy-dispersive X-ray spectrometer (EDX; X-Max 20 mm², Oxford, UK) were used. The photocatalysis absorbance spectra were measured by a UV-visible spectrophotometer (V-630, JASCO, Lisses, France) with a wavelength range of 250–650 nm. The chemical compositions of the prepared powders were characterized by infrared (IR) spectroscopy (Bruker II-RAM, Karlsruhe, Germany). UV lamp (VL-4LC, 4W-254 nm) was used to activate the photodegradation.

3.3. Sample Preparation

3.3.1. Preparation of Powders

Two methods were used for the preparation of powders: the traditional mixture and the co-precipitation (see Appendix A). In the first method, the DD3 and DD3 + 38 wt% ZrO₂ kaolinitic clay powders were mixed using a mill with different contents of ZnO (0, 10, 25, and 50 wt%), and 5.37 wt% CuO. The addition of ZrO₂ to DD3 was used to obtain a ceramic composed of mullite and zircon, after sintering for 2 h at 1300 °C. The average particle size of the added ZnO powder was about 1 μm, as indicated by the supplier.

The second performed method was co-precipitation. It is noted that in this method, various amounts of zinc acetate and copper (28, 2.8/ 25 and 12.5 wt%) were added into the same clay. Copper and zinc acetates were dissolved in a sodium hydroxide solution previously diluted in distilled water (0.5 M).

3.3.2. The Photocatalytic Activity Measurement

The photocatalytic activity of all the materials was measured by monitoring the absorbance evolution of a dye-containing solution. After preparation of the aqueous solution with orange II (25 mg/l; pH = 8.9), 1 g of the studied powder was dispersed in 25 mL of this dye solution. In order to activate the reaction between the powder and the solution, the obtained mixture was deposited on a shaker (stirring 500 R/min) in a dark room. Then, a lamp (VL-4LC, 4 W-254 nm) was used as a light source to activate the reaction). After each 15 min, 2.2 mL of the solution was placed in a sealed tube and centrifuged at 3500 U/min during 7 min in order to remove the catalyst. The solution was analyzed by measuring the UV-Vis absorbance spectra in the wavelength range of 250–650 nm. Distilled water was used as a reference and measurements of the catalyst solution were carried out every 15 min. The absorption rate of degradation is calculated using the following equation [61]:

$$\text{Degradation ratio} = \frac{C_0 - C}{C_0} \times 100\% \quad (3)$$

where C₀ and C are the initial concentration before and after illumination, respectively.

4. Conclusions

The photocatalytic degradation of a dye solution by different ceramic powders prepared by two different methods including the co-precipitation and traditional mixing showed a great effect on the photocatalytic activity. The material is based on a DD3 material with or without ZrO_2 and different oxides (ZnO and CuO). This dye degradation was done with and without a UV-lamp on powders where the ceramic material was dominant. The powders were used as catalysts. A very high rate of orange II degradation reached 93.63% after a short period of 15 min with DD3 +14.28 wt% ZnO + 5.37wt% CuO, and DD3Z + 14.28 wt% ZnO + 5.37wt% CuO. For these additions, the morphology of the grains became more porous with flake like structures. In this study, the chemical reactions of the added oxides coupled with the method of preparation have shown that the degradation of the dye was considerably improved. The results of the photocatalytic degradation of the OII dye solution by different ceramic powders are compared with thin films of the same materials. Ceramic powders induce a photodegradation that can be 5 to 10 times faster than thin films.

Author Contributions: Conceptualization, M.Z. and A.M.; methodology, A.h.M.; writing—original draft preparation, D.B. and R.B.; writing—review and editing, R.B.; visualization, A.H.; project administration, funding acquisition, M.Z. All authors have read and agreed to the published version of the manuscript.

Funding: This research received no external funding.

Acknowledgments: This work has been supported by the Laboratory of active components and materials University Larbi Ben M'hidi Oum El Bouaghi, Algeria, and laboratory of MOLTECH-Anjou, University of Angers, France. All thanks and gratitude to the Belkacem Bouricha Karima teacher of English at the same university for her assistance.

Conflicts of Interest: The authors declare no conflict of interest.

Appendix A

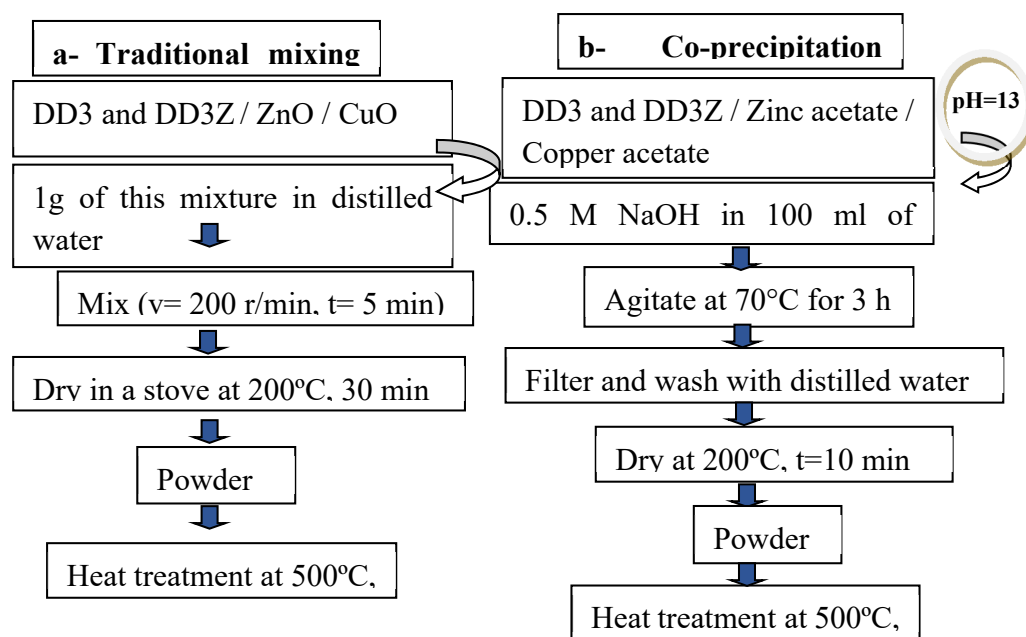
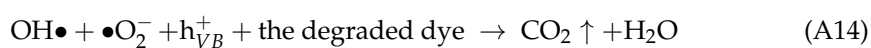
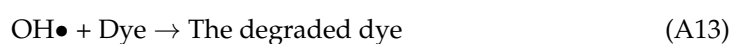
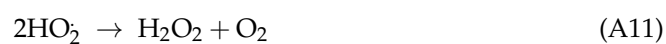
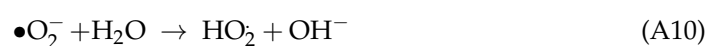
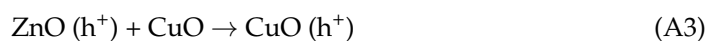
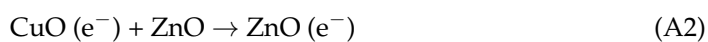
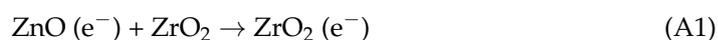


Figure A1. The two methods followed for the preparation of powders.

Appendix B

The following reactions are also present:



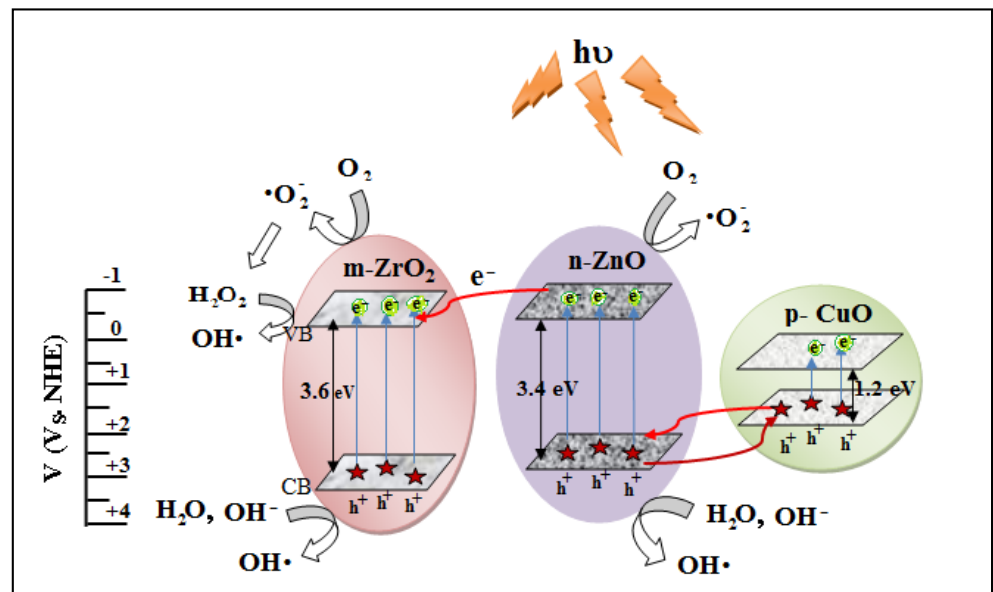


Figure A2. The photocatalytic composite mechanism $ZrO_2/CuO/ZnO$ under UV light.

Appendix C

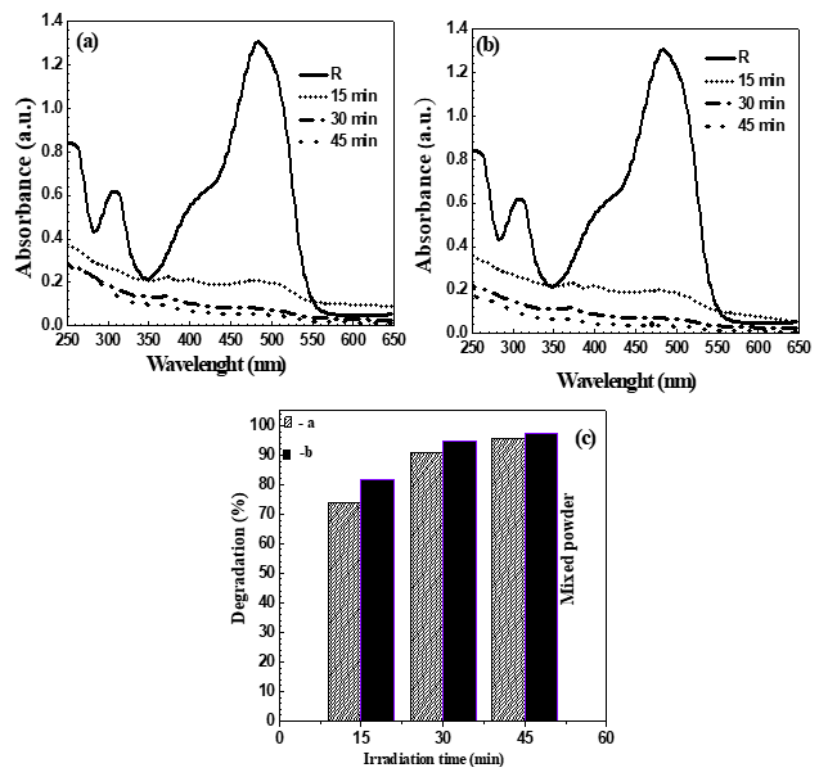


Figure A3. Percentage change of orange II degradation versus time without lamp for ceramic powders prepared by traditional mix method, (a) DD3 + 14.28 wt% ZnO + 5.37 wt% CuO and (b) DD3Z + 14.28 wt% ZnO + 5.37 wt% CuO, (c) bar graph of the results for the two materials. R = reference value for OII.

Appendix D

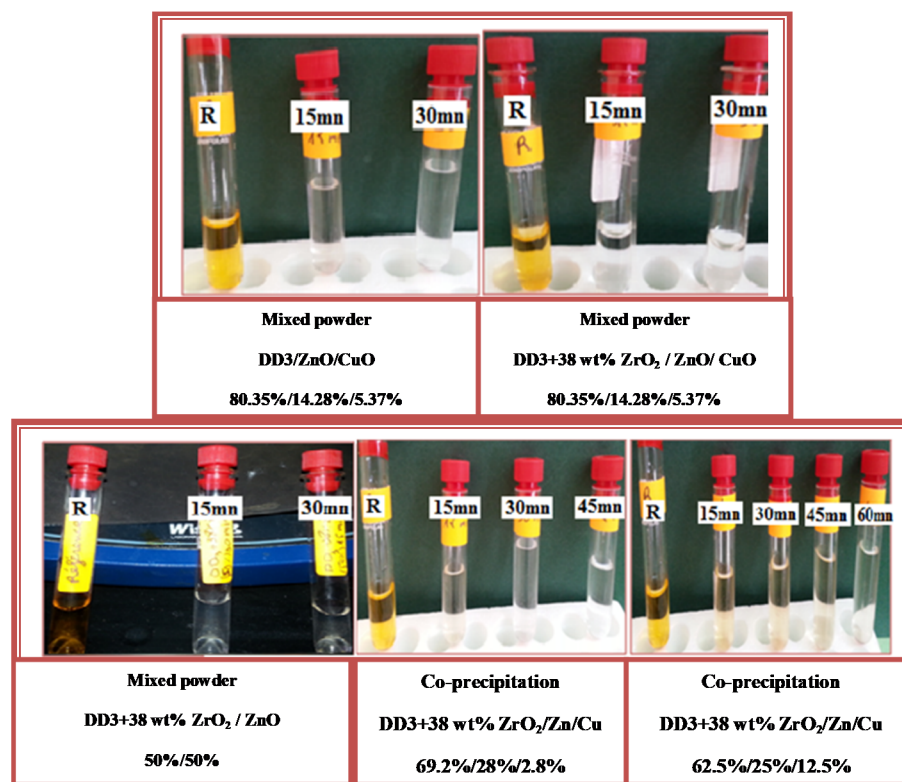


Figure A4. Image showing the discoloration of OII for different durations of exposure under UV light.

Appendix E

Table A1. Results of structural analyses of type DD3 before and after addition (Zn: Cu).

Phases	Plan (hkl)	2 θ (°)	θ (°)	FHWM β (°)	β (rad)	D (nm)
Mullite	(210)	26.278	13.139	0.356	0.0062	22
Mullite + + 25% Zn + 12.5%Cu	(210)	26.311	13.155	0.593	0.0103	13
Mullite + 28% Zn + 2.8%Cu	(210)	26.118	13.059	0.605	0.0105	13
SiO ₂	(101)	21.680	10.84	0.261	0.0045	31
SiO ₂ + 25% Zn + 12.5%Cu	(101)	21.707	10.853	0.353	0.00616	22
SiO ₂ + 28% Zn + 2.8%Cu	(101)	21.54	10.77	0.373	0.0065	21

Table A2. Results of structural analyses of type DD3 + 38% ZrO₂ before and after addition (Zn: Cu).

Phases	Plan (hkl)	2θ (°)	θ (°)	FHWM β(°)	β(rad)	D (nm)
Mullite	(121)	40.821	20.41	0.382	0.0067	22
Mullite + 25% Zn + 12.5%Cu	(121)	40.889	20.444	0.532	0.0093	15
Mullite + 28% Zn + 2.8%Cu	(121)	41.071	20.535	0.675	0.0118	12
ZrSiO ₄	(200)	27.017	13.508	0.188	0.0033	43
ZrSiO ₄ + 25% Zn + 12.5%Cu	(200)	27.068	13.534	0.468	0.0082	17
ZrSiO ₄ + 28% Zn + 2.8%Cu	(200)	27.217	13.608	0.656	0.0114	12
SiO ₂	(101)	21.667	10.833	0.246	0.0043	32
SiO ₂ + 25% Zn + 12.5%Cu	(101)	21.737	10.868	0.47	0.0082	17
SiO ₂ + 28% Zn + 2.8%Cu	(101)	21.92	10.96	0.623	0.0109	12
ZrO ₂	(−111)	28.196	14.098	0.209	0.0036	39
ZrO ₂ + 25% Zn + 12.5%Cu	(−111)	28.289	14.144	0.468	0.0082	17
ZrO ₂ + 28% Zn + 2.8%Cu	(−111)	28.441	14.220	0.606	0.0106	13.489

References

- Seabra, M.P.; Pires, R.R.; Labrincha, J.A. Ceramic tiles for photodegradation of Orange II solutions. *Chem. Eng. J.* **2011**, *171*, 692–702. [\[CrossRef\]](#)
- Yang, H.; Xu, S.; Chitwood, D.E.; Wang, Y. Ceramic water filter for point-of-use water treatment in developing countries: Principles, challenges and opportunities. *Front. Environ. Sci. Eng.* **2020**, *14*, 79. [\[CrossRef\]](#)
- Harabi, A.; Zenikheri, F.; Boudaira, B.; Bouzerara, F.; Guechi, A.; Foughali, L. A new and economic approach to fabricate resistant porous membrane supports using kaolin and CaCO₃. *J. Eur. Ceram. Soc.* **2014**, *34*, 1329–1340. [\[CrossRef\]](#)
- Kouras, N.; Harabi, A.; Bouzerara, F.; Foughali, L.; Policicchio, A.; Stelitano, S.; Galiano, F.; Figoli, A. Macro-porous ceramic supports for membranes prepared from quartz sand and calcite mixtures. *J. Eur. Ceram. Soc.* **2017**, *37*, 3159–3165. [\[CrossRef\]](#)
- Bouzerara, F.; Boulanacer, S.; Harabi, A. Shaping of microfiltration (MF) ZrO₂ membranes using a centrifugal casting method. *Ceram. Inter.* **2015**, *41*, 5159–5163. [\[CrossRef\]](#)
- Otitojua, T.A.; Okoyeb, P.U.; Chend, G.; Lia, Y.; Okoyec, M.O.; Li, S. Advanced ceramic components: Materials, fabrication, and applications. *J. Ind. Eng. Chem.* **2020**, *85*, 34–65. [\[CrossRef\]](#)
- Harabi, A.; Karboua, N.; Achour, S. Effect of thickness and orientation of alumina fibrous thermal insulation on microwave heating in a modified domestic 2.45 GHz multi-mode cavity. *Int. J. Appl. Ceram. Technol.* **2012**, *9*, 124–132. [\[CrossRef\]](#)
- Harabi, E.; Harabi, A.; Mezahi, F.Z.; Zouai, S.; Karboua, N.; Chehalatt, S. Effect of P₂O₅ on mechanical properties of porous natural hydroxyapatite derived from cortical bovine bones sintered at 1050 °C. *Des. Wat. Treat.* **2016**, *57*, 5297–5302. [\[CrossRef\]](#)
- Ghouil, B.; Harabi, A.; Bouzerara, F. Elaboration and characterization of ceramic membrane supports from raw materials used in microfiltration. *Des. Wat. Treat.* **2016**, *57*, 5241–5245. [\[CrossRef\]](#)
- Foughali, L.; Harabi, A.; Barama, S.E.; Bouzerara, F.; Guechi, A.; Boudaira, B. Effect of sodium phosphate additions on mechanical properties of porous Sigue quartz sand. *Des. Wat. Treat.* **2016**, *57*, 5286–5291. [\[CrossRef\]](#)
- Ghouil, B.; Harabi, A.; Bouzerara, F.; Boudaira, B.; Guechi, A.; Demir, M.M.; Figoli, A. Development and characterization of tubular composite ceramic membranes using natural alumino-silicates for microfiltration applications. *Mat. Charact.* **2015**, *103*, 18–27. [\[CrossRef\]](#)
- Mdjemem, N.; Harabi, A.; Bouzerara, F.; Foughali, L.; Boudaira, B.; Guechi, A.; Brihi, N. Elaboration and characterization of low cost ceramics microfiltration membranes applied to the sterilization of plant tissue culture media. *J. Taiwan Inst. Chem. Eng.* **2016**, *59*, 79–85. [\[CrossRef\]](#)
- Harabi, A.; Kasrani, S.; Foughali, L.; Benhassine, M.T.; Kitouni, S. Effect of TiO₂ additions on densification and mechanical properties of new mullitiform resistant porcelains using economic raw materials. *Ceram. Inter.* **2017**, *43*, 5547–5556. [\[CrossRef\]](#)

14. Harabi, E.; Harabi, A.; Foughali, L.; Chehlatt, S.; Zouai, S.; Mezahi, F.Z. Grain growth in sintered natural hydroxyapatite. *Acta Phys. Pol. A* **2015**, *127*, 1161–1163. [[CrossRef](#)]
15. Boudaira, B.; Harabi, A.; Bouzerara, F.; Zenikheri, F.; Guechi, A. Preparation and characterization of membrane supports for microfiltration and ultrafiltration using kaolin (DD2) and CaCO₃. *Des. Wat. Treat.* **2016**, *57*, 5258–5265. [[CrossRef](#)]
16. Chehlatt, S.; Harabi, A.; Oudadesse, H.; Harabi, E. In Vitro Bioactivity Study of Pure Wollastonite Prepared from Local Raw Materials. *Acta Phys. Pol. A* **2015**, *127*, 925–927. [[CrossRef](#)]
17. Ma, J.; Wang, K.; Li, L.; Zhang, T.; Kong, Y.; Komarneni, S. Visible-light photocatalytic decolorization of Orange II on Cu₂O/ZnO nanocomposites. *Ceram. Int.* **2015**, *41*, 2050–2056. [[CrossRef](#)]
18. Siuleiman, S.; Kaneva, N.; Bojinova, A.; Papazova, K.; Apostolov, A.; Dimitrov, D. Photodegradation of Orange II by ZnO and TiO₂ powders and nanowire ZnO and ZnO/TiO₂ thin films. *Colloids Surf. A Physicochem. Eng. Aspects* **2014**, *460*, 408–413. [[CrossRef](#)]
19. Mecif, A.; Soro, J.; Harabi, A.; Bonnet, J.P. Preparation of Mullite- and Zircon-Based Ceramics Using Kaolinite and Zirconium Oxide: A Sintering Study. *J. Am. Ceram. Soc.* **2010**, *93*, 1306–1312. [[CrossRef](#)]
20. Witoon, T.; Permsirivanich, T.; Chareonpanich, M. Chitosan-assisted combustion synthesis of CuO–ZnO nanocomposites: Effect of pH and chitosan concentration. *Ceram. Int. J.* **2013**, *39*, 3371–3375. [[CrossRef](#)]
21. Ezeigwe, E.R.; Tan, M.T.T.; Khiew, P.S.; Siong, C.W. One-step green synthesis of graphene/ZnO nanocomposites for electrochemical capacitors. *Ceram. Int. J.* **2015**, *41*, 715–724. [[CrossRef](#)]
22. Marto, J.; São Marcos, P.; Trindade, T.; Labrincha, J.A. Photocatalytic decolouration of Orange II by ZnO active layers screen-printed on ceramic tiles. *J. Hazard. Mater.* **2009**, *163*, 36–42. [[CrossRef](#)]
23. Huang, J.; Dai, Y.; Gu, C.; Sun, Y.; Liu, J. Preparation of porous flower-like CuO/ZnO nanostructures and analysis of their gas-sensing property. *J. Alloys Comp.* **2013**, *575*, 115–122. [[CrossRef](#)]
24. Zaman, S. *Synthesis of ZnO, CuO and Their Composite Nanostructures for Optoelectronics, Sensing and Catalytic Applications*; Linköping University, in Science and Technology: Linköping, Sweden, 2012. [[CrossRef](#)]
25. Kanade, K.G.; Kale, B.B.; Baeg, J.O.; Lee, S.M.; Lee, C.W.; Moon, S.J.; Chang, H. Self-assembled aligned Cu doped ZnO nanoparticles for photocatalytic hydrogen production under visible light irradiation. *Mater. Chem. Phys.* **2007**, *102*, 98–104. [[CrossRef](#)]
26. Sathishkumar, P.; Sweena, R.; Wu, J.J.; Anandan, S. Synthesis of CuO-ZnO nanophotocatalysts for visible light assisted degradation of a textile dye in aqueous solution. *Chem. Eng. J.* **2011**, *171*, 136–140. [[CrossRef](#)]
27. Thaweesaeng, N.; Supankit, S.; Techidheera, W.; Pecharapa, W. Structure properties of as-synthesized Cu-doped ZnO nanopowder synthesized by co-precipitation method. *Eng. Procedia* **2013**, *34*, 682–688. [[CrossRef](#)]
28. Shao, B.; Qiu, J.H.; Zhu, K.J.; Cao, Y.; Ji, H.L. Effect of CuO on dielectric and piezoelectric properties of (K_{0.4425}Na_{0.52}Li_{0.0375})(Nb_{0.87}Ta_{0.06}Sb_{0.07})O₃ ceramics. *J. Alloys Compd.* **2012**, *515*, 128–133. [[CrossRef](#)]
29. Jurado, L.T.; Hernández RM, A.; Rangel, E. Sol-Gel synthesis of mullite starting from different inorganic precursors. *J. Powder Technol.* **2013**, *7*. [[CrossRef](#)]
30. Vempati, R.K.; Rao, A.; Hess, T.R.; Cocke, D.L.; Lauer, H.V., Jr. Fractionation and characterization of texas lignite class 'F' fly ash by XRD, TGA, FTIR and SFM. *Cement Concr. Res.* **1994**, *24*, 1153–1164. [[CrossRef](#)]
31. Gougazeha, M.; Buhl, J.-C. Synthesis and characterization of zeolite A bihydrothermal transformation of natural Jordanian kaolin. *JAAU Basic Appl. Sci.* **2014**, *15*, 35–42. [[CrossRef](#)]
32. Zhang, M.; Salje, E.K.H. Infrared spectroscopic analysis of zircon: Radiation damage and the metamict state. *J. Phys. Condens. Matter.* **2001**, *13*, 3057–3071. [[CrossRef](#)]
33. Agorku, E.S.; Kuvarega, A.T.; Mamba, B.B.; Pandey, A.C.; Mishra, A.K. Enhanced visible-light photocatalytic activity of multi-elements-doped ZnO for degradation of indigo carmine. *J. Rare Earths* **2015**, *33*, 498. [[CrossRef](#)]
34. Habibi, M.H.; Karimi, B. Application of impregnation combustion method for fabrication of nanostructure CuO/ZnO composite oxide: XRD, FESEM, DRS and FTIR study. *J. Ind. Eng. Chem.* **2014**, *20*, 1566–1570. [[CrossRef](#)]
35. Lellis, B.; Fávoro-Polonio, C.Z.; Pamphile, J.A.; Polonio, J.C. Effects of textile dyes on health and the environment and bioremediation potential of living organisms. *Biotechnol. Res. Innov.* **2019**, *3*, 275–290. [[CrossRef](#)]
36. Bandara, J.; Herrera, F.G.; Kiwi, J.T.; Pulgarin, C.O. Degradation of concentrated-solutions of non-biodegradable orange-ii by photocatalytic and electrochemical methods. *J. Chem. Res.* **1998**, 234. [[CrossRef](#)]
37. Qiu, R.; Zhang, D.; Mo, Y.; Song, L.; Brewer, E.; Huang, X.; Xiong, Y. Photocatalytic activity of polymer-modified ZnO under visible light irradiation. *J. Hazard. Mater.* **2008**, *156*, 80–85. [[CrossRef](#)]
38. Poullos, I.; Micropoulou, E.; Panou, R.; Kostopoulou, E. Photooxidation of eosin Y in the presence of semiconducting oxides. *Appl. Catal. B* **2003**, *41*, 345–355. [[CrossRef](#)]
39. Novikov, S.; Timoshcnkov, S. Long-range electrostatic forces on the surfaces of aluminum oxide and silica oxide'. *Adv. Colloid Interface Sci.* **2003**, *105*, 341–353. [[CrossRef](#)]
40. Zhang, C.; Chen, H.; Ma, M.; Yang, Z. Facile synthesis of magnetically recoverable Fe₃O₄/Al₂O₃/molecularly imprinted TiO₂ nanocomposites and its molecular recognitive photocatalytic degradation of target contaminant. *Mol. Catal. A Chem.* **2015**, *402*, 10–16. [[CrossRef](#)]
41. Fu, X.; Tang, W.; Ji, L.; Chen, S. V₂O₅/Al₂O₃ composite photocatalyst: Preparation, characterization, and the role of Al₂O₃. *Chem. Eng. J.* **2012**, *180*, 170–177. [[CrossRef](#)]

42. Bansal, P.; Chaudhary, G.R.; Mehta, S.K. Comparative study of catalytic activity of ZrO₂ nanoparticles for sonocatalytic and photocatalytic degradation of cationic and anionic dyes. *Chem. Eng. J.* **2015**, *280*, 475–485. [[CrossRef](#)]
43. Sheini, F.J.; Singh, J.; Srivasatva, O.N.; Joag, D.S.; More, M.A. Electrochemical synthesis of Cu /ZnO nanocomposite films and their efficient field emission behaviour. *Appl. Surf. Sci.* **2010**, *256*, 2110–2114. [[CrossRef](#)]
44. Tan, G.; Huang, J.; Zhang, L.; Ren, H.; Xia, A. An enhanced visible-light-driven photocatalyst: Conduction band control of Bi₂WO₆ crystallites by Cu ion modification. *Ceram. Int.* **2014**, *40*, 11671–11679. [[CrossRef](#)]
45. Saravanana, R.; Karthikeyan, S.; Gupta, V.K.; Sekaran, G.; Narayanane, V.; Stephen, A. Enhanced photocatalytic activity of ZnO/CuO nanocomposite for the degradation of textile dye on visible light illumination. *Mat. Sci. Eng. C* **2013**, *33*, 91–98. [[CrossRef](#)] [[PubMed](#)]
46. Sakib, A.A.M.; Masum, S.M.; Hoinkis, J.; Islam, R.; Molla, M.A.I. Synthesis of CuO/ZnO Nanocomposites and Their Application in Photodegradation of Toxic Textile Dye. *J. Compos. Sci.* **2019**, *3*, 91. [[CrossRef](#)]
47. Basahel, S.N.; Ali, T.T.; Mokhtar, M.; Narasimharao, K. Influence of crystal structure of nanosized ZrO₂ on photocatalytic degradation of methyl orange. *Nanoscale Res. Lett.* **2015**, *10*, 73. [[CrossRef](#)]
48. Katal, R.; Masudy-Panah, S.; Kongb, E.Y.-J.; Dasineh Khiaviv, N.; Davood, M.H.; Farahanid, A.; Gong, X. Nanocrystal-engineered thin CuO film photocatalyst for visible-light-driven photocatalytic degradation of organic pollutant in aqueous solution. *Catal. Today* **2020**, *340*, 236–244. [[CrossRef](#)]
49. Al-Ghamdi, A.A.; Khedr, M.H.; Ansari, M.S.; Hasan PM, Z.; Abdel-Wahab, M.S.; Farghali, A.A. RF sputtered CuO thin films: Structural, optical and photo-catalytic behavior. *Phys. E* **2016**, *81*, 83–90. [[CrossRef](#)]
50. Nezamzadeh-Ejhieh, A.; Karimi-Shamsabadi, M. Comparison of photocatalytic efficiency of supported CuO onto micro and nano particles of zeolite X in photodecolorization of Methylene blue and Methyl orange aqueous mixture. *Appl. Catal. A Gen.* **2014**, *477*, 83–92. [[CrossRef](#)]
51. Fraile, J.M.; Le Jeune, K.; Mayoral, J.A.; Ravasio, N.; Zaccheri, F. CuO/SiO₂ as a simple, effective and recoverable catalyst for alkylation of indole derivatives with diazocompounds. *Org. Biomol. Chem.* **2013**, *11*, 4327. [[CrossRef](#)]
52. Khiavi, N.D.; Katal, R.; Eshkalak, S.K.; Masudy-Panah, S.; Ramakrishna, S.; Jianguyong, H. Visible Light Driven Heterojunction Photocatalyst of CuO–Cu₂O Thin Films for Photocatalytic Degradation of Organic Pollutants. *Nanomaterials* **2019**, *9*, 1011. [[CrossRef](#)] [[PubMed](#)]
53. Singha, J.; Mannab, A.K.; Sonia, R.K. Sunlight driven photocatalysis and non-enzymatic glucose sensing performance of cubic structured CuO thin films. *Appl. Surf. Sci.* **2020**, *530*, 147258. [[CrossRef](#)]
54. Das, S.; Srivastava, V.C. An overview of the synthesis of CuO-ZnO nanocomposite for environmental and other applications. *Nanotechnol. Rev.* **2018**, *7*, 267–282. [[CrossRef](#)]
55. Paz, D.S.; Foletto, E.L.; Bertuol, D.A.; Jahn, S.L.; Collazzo, G.C.; da Silva, S.S.; Chiavone-Filho, O.; do Nascimento, C.A.O. CuO/ZnO coupled oxide films obtained by the electrodeposition technique and their photocatalytic activity in phenol degradation under solar irradiation. *Water Sci. Tech.* **2013**, *68*, 5. [[CrossRef](#)] [[PubMed](#)]
56. Qamar, M.T.; Aslam, M.; Ismail, I.M.I.; Salah, N.; Hameed, A. Synthesis, Characterization, and Sunlight Mediated Photocatalytic Activity of CuO Coated ZnO for the Removal of Nitrophenols. *ACS Appl. Mater. Interfaces* **2015**, *7*, 8757–8769. [[CrossRef](#)] [[PubMed](#)]
57. Jothibas, M.; Manoharan, C.; Jeyakumar, S.J.; Praveen, P.; Panneerdoss, I.J. Photocatalytic activity of spray deposited ZrO₂ nano-thin films on methylene blue decoloration. *J. Mater. Sci. Mater. Electron.* **2016**, *27*, 5851–5859. [[CrossRef](#)]
58. Poliseti, S.; Deshpande, P.A.; Madras, G. Photocatalytic Activity of Combustion Synthesized ZrO₂ and ZrO₂/TiO₂ Mixed Oxides. *Ind. Eng. Chem. Res.* **2011**, *50*, 12915–12924. [[CrossRef](#)]
59. Majedi, A.; Davar, F.; Abbasi, A.; Ashrafi, A. Modified Sol–Gel Based Nanostructured Zirconia Thin Film: Preparation, Characterization, Photocatalyst and Corrosion Behavior. *J. Inorg. Organomet. Polym.* **2016**, *26*, 932–942. [[CrossRef](#)]
60. Bouras, D.; Mecif, A.; Barillé, R.; Harabi, A.; Rasheed, M.; Mahdjoub, A.; Zaabat, M. Cu:ZnO deposited on porous ceramic substrates by a simple thermal method for photocatalytic application. *Ceram. Int.* **2018**, *44*, 21546–21555. [[CrossRef](#)]
61. Ajmal, A.; Riffat, I.M.; Malik, N.; Idriss, H.; Nadeem, M.A. Principles and mechanisms of photocatalytic dye degradation on TiO₂ based photocatalysts: A comparative overview. *RSC Adv.* **2014**, *4*, 37003–37026. [[CrossRef](#)]